PASJ: Publ. Astron. Soc. Japan , 1–??,

Modeling Non-Potential Magnetic Fields in NOAA Active Region 10930 as Observed by Hinode XRT

Monica G. Bobra[1] A. van Ballegooijen[1] E. DeLuca[1] R. Kano[2] K. Korreck[1] N. Narukage[2] T. Sakao[2] K. Shibasaki[3] Y. Su[1,4]

[1]*Harvard-Smithsonian Center for Astrophysics, 60 Garden Street, Cambridge MA 02138*

[2]*National Astronomical Observatory, Mitaka, Tokyo 181-8588, Japan*

[3]*National Astronomical Observatory, Nobeyama, Minamimaki, Minamisaku, 384-1305 Nagano, Japan*

[4]*Purple Mountain Observatory, Nanjing, China; and Graduate University of Chinese Academy of Sciences, China*

(Received 2000 December 31; accepted 2001 January 1)

Abstract

Many models aim to reproduce the non-linear force free fields in the solar corona; in this particular study, the magnetofrictional relaxation method is used. This method produces non-linear force free fields in and around an active region filament. The method is based on line-of-sight magnetograms and ground-based Hα images to define the location of a filament, which is represented by a flux rope.

In this paper, we describe one such model that qualitatively reproduces *Hinode* X-Ray Telescope (XRT) observations of highly sheared, non-potential loop structures in NOAA Active Region 10930, which occured on 12 December 2006. We find that a flux rope with an axial flux of 10^{21} Maxwells is needed to reproduce the observed loops. We also derive estimates of the current, torsion parameter α, and quasi-separatrix layer distribution, as well as the relative magnetic helicity and magnetic free energy.

Key words: Sun: corona; Sun: magnetic fields

1. Introduction

It is generally agreed that solar flares represent the release of magnetic free energy stored in the corona prior to the flare (Priest & Forbes 2002). The study of solar flares and other eruptive phenomena requires that we understand the 3D structure of the pre-flare coronal magnetic field configuration and the physical processes that cause the field to become unstable. At present, the details of the configuration are not well understood, so it is difficult to determine the causes of instability. Twisted or sheared magnetic fields are often visible in the solar corona before solar flares erupt (Rust & Kumar 1996; Canfield et al. 1999; Sterling et al. 2000) but it is unclear exactly what triggers their eruption.

An example of highly sheared field is the region in and around active region filaments. The mass of the plasma contained in filaments may be supported by a highly sheared, weakly twisted flux rope lying horizontally above the polarity inversion line (PIL) (Kuperus & Raadu 1974; Pneuman 1983; Priest et al. 1989; van Ballegooijen & Martens 1989; Rust & Kumar 1994; Low & Hundhausen 1995; Chae et al. 2001). In this study, we aim to model such twisted field lines in and around the filament in NOAA Active Region 10930 in order to understand the causes of the ensuing X-Class flare.

We compare the results of our model with the highly sheared field visible in *Hinode* XRT data. XRT is an ideal instrument for this study because it can resolve individual sheared loops in hot plasmas, where shear is most likely to occur, thus putting stronger observational constraints on magnetic field models than EUV data (Bobra et al. 2007).

2. Model

The magnetic pressure in the corona is generally much larger than the gas pressure ($\beta = 8\pi p/B^2 \ll 1$), so magnetic forces are dominant. Therefore, except during an eruption, the magnetic field $\mathbf{B}(\mathbf{r})$ is nearly force free; i.e. $\mathbf{j} \times \mathbf{B} \approx 0$, where $\mathbf{j}(\mathbf{r})$ is the electric current density. There are two classes of solutions for the equation $\mathbf{j} \times \mathbf{B} = 0$, or $(\nabla \times \mathbf{B}) \times \mathbf{B} = 0$. A linear force free field solution satisfies $\nabla \times \mathbf{B} = \alpha \mathbf{B}$, where α is constant. A non-linear force free solution satisfies $\nabla \times \mathbf{B} = \alpha(\mathbf{r})\mathbf{B}$, where the value of α varies among different field lines yet is constant for any particular field line.

While linear force free solutions are analytic and require little computing time, the constant-α prevents such solutions from accurately modeling sheared fields. In addition, since sheared fields store free energy, linear force free models cannot produce accurate estimates of helicity and free energy. To accurately model sheared fields and obtain reasonable helicity and free energy estimates, one must use a non-linear force free field (NLFFF) model (van Ballegooijen 2004). In addition, the value of α in and around such a flux rope varies greatly with position. Therefore, to accurately model active region filaments, one must use NLFFF models.

In this study, a non-linear force-free field (NLFFF) model of AR 10930 was constructed on the basis of a longitudinal magnetogram. The method involves computing a potential field model and inserting a (non-force-free) magnetic flux rope at the location of an observed Hα filament. Finally magneto-frictional relaxation is applied by solving the ideal MHD induction equation

$$\frac{\partial \mathbf{A}}{\partial t} = \mathbf{v} \times \mathbf{B}, \quad (1)$$

where $\mathbf{v}$ is the plasma velocity. In the magneto-frictional method, the velocity is assumed to be proportional to the Lorentz force, $\mathbf{v} = \nu^{-1}\mathbf{j} \times \mathbf{B}/B^2$, where ν is the friction coefficient. The boundary conditions are such that the horizontal components of $\mathbf{A}(\mathbf{r})$ on the photosphere are held fixed during the iteration process, so the radial magnetic field at the photosphere remains unchanged. We also use periodic boundary conditions in longitude, closed boundaries in latitude, and open boundary conditions at the top, where the field is assumed to be radial.

The latest version of the code takes into account deviations from force-free conditions in the photosphere (see Metcalf et al. 2007), and includes hyper-diffusion in the corona to suppress artifacts in the coronal current distribution (for details see Bobra et al. (2007)). The final configuration is compared with both Hα observations of the filament and XRT observations of the surrounding corona.

3. Observations

Three sets of observational data were used in this study (dates and times of each observation are listed in Table 1): The line-of-sight component from a magnetogram taken by the Kitt Peak SOLIS Vector Spectromagnetograph, full-disk Hα image from Kanzelhöhe Observatory, and Soft X-Ray images taken by the Hinode X-Ray Telescope, which has 1″ pixels or an angular resolution of 2″ (Golub et al. 2007). These data represent the solar magnetic field configuration at the photosphere, chromosphere, and corona, respectively.

The X-Ray image is shown in the top panel of Figure 1. Soft X-Ray images observed by *Yohkoh* SXT showed S-shaped structures called *sigmoids*; *Hinode* XRT observations resolve such sigmoids into multiple, thin sheared loops that display both continuous and discontinuous S-structures.

4. Results

Figure 1 shows a model constructed with a flux rope that has an axial flux of 10^{21} Mx and a poloidal flux of -10^{11} Mx/cm (left-helical twist) from two angles separated by 90°. Such a flux rope qualitatively reproduces the individual S-shaped sheared loops seen in the active region core as seen by XRT.

The model parameters are listed in Table 1. The axial flux, free energy, ratio of free energy and potential field energy, and helicity indicate values that will produce a solution that matches observations. The twist angle $\theta = |2\pi(F_{pol}L)(\Phi_{axi})^{-1}|$, where L is the length of the flux rope.

Canfield et al. (1999) found that active regions containing sigmoids are likely to erupt. Our non-linear force-free model of multiple sigmoidal loops produces $\approx 10^{32}$ ergs of free energy, which is ≈60% of the potential field energy. Such a result suggests that multiple sigmoidal loops as observed by XRT contain a significant amount of energy, which is consistent with eruptive behavior. In addition, our model finds the associated flux rope has a twist of 13.7 radians, which is far above the threshold for eruption, commonly believed to be $\approx 2\pi$ radians (Hood & Priest 1981; Török et al. 2004).

Table 1. Flux Rope Parameters. [a]Below, these coordinates are given in(Latitude, Central Meridian Distance).[b]The computational domain is represented in spherical coordinates; above, these coordinates have been translated into average x and y values in arcseconds.

XRT Data Time	12-12-2006 16:12:57 UT
Hα Data Time	12-12-2006 07:49:45 UT
SOLIS Data Time	12-12-2006 16:13:00 UT
Active Region Number	NOAA 10930
Domain center[a]	(20.1, -6.7)
Resolution $\delta\phi$	0.0015 radians
Domain Size(″)[b]	512×512
Flux Imbalance	-2.20 Gauss
Length of Flux Rope	218,000 km
Poloidal Flux	-10^{11} Mx/cm
Potential field (PF) energy	5.04×10^{32} erg
Axial Flux	10^{21} Mx
Twist angle θ	13.7 radians
Free Energy	2.93×10^{32} erg
Free Energy (% of PF)	58
Relative Helicity	-1.77×10^{43} (Mx^2)

We determined the 3-D current distribution from $\mathbf{j} = \nabla \times \mathbf{B}$. A plot of the vertical component of the current density at a height of $z = 4$, which corresponds to the center of the flux rope, is shown in the top panel of Figure 2. The yellow line represents the x-axis of the image below, which shows the current distribution along a cross-section of the flux rope, looking towards the West. White lines represent selected magnetic field lines from the model's result. It is worth noting that the right-most magnetic field line, which looks like it is looping over itself, is actually a sheared line traveling along the axis of the flux rope. We find that this magnetic field configuration is consistent with those described in Karpen et al. (2005), whom suggest that such long, horizontal field lines can support the weight of a filament.

The current distribution is zero throughout most of the domain and peaks at the location of the flux rope. This is to be expected, due to the formation of current sheets during the flux rope insertion process. However the presence of a flux rope in the solar atmosphere will likely have associated current sheets and thus the distribution is realistic.

Figure 3 shows the quasi-separatrix layers (QSL) for a potential field model of AR 10930 (top panel) and for the non-linear force free model (bottom panel). Each figure shows the plane $z = 4$ of the computational volume divided into three areas. Magnetic field lines in the blue area have both footpoints in the computational volume. The brightness in the blue area is proportional to the function

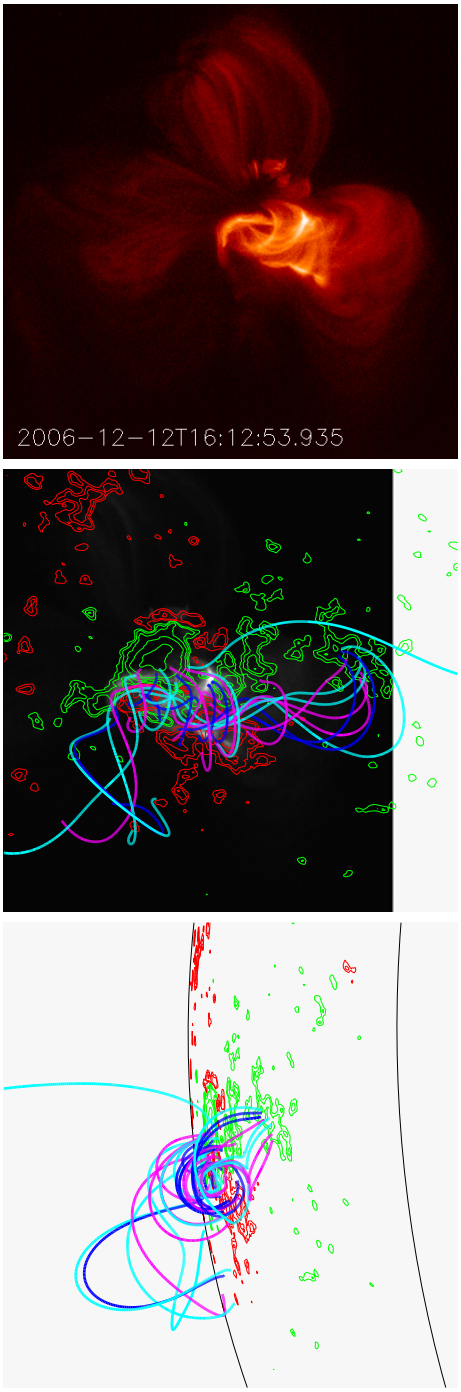

Fig. 1. Top: An XRT image taken on 12 December 2006 at 16:12:54 with the Aluminum-Poly filter. Middle: The XRT image and photospheric flux distribution overlaid with selected field lines from our model. Bottom: The same field lines rotated by 90°.

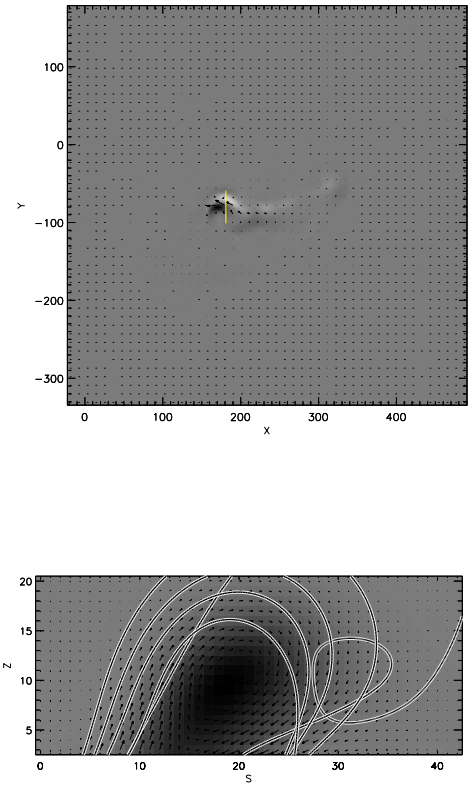

Fig. 2. Top: A plot of the current distribution at a height of $z = 4$, in the x-y plane. Bottom: The same current distribution in an s-z plane, where s is the yellow line in the top image.

$$N(x,y) = \sqrt{\sum_{i=1,2}\left[\left(\frac{\partial X_i}{\partial x}\right)^2 + \left(\frac{\partial X_i}{\partial y}\right)^2\right]}, \qquad (2)$$

where (x, y) is the starting point of a field line, (x', y') and (x'', y'') are the two end points, and $\{X_1, X_2\}$ define a vector $\{x'' - x', y'' - y'\}$ (Titov & Démoulin 1999). Field lines in the brown area intersect the sides of the computational volume. Field lines in the green area intersect the top of the computational volume. The QSL calculation was performed only in the blue area.

The QSL map is plotted at a height of 4 grid cells, or 5.5 Mm, above the photosphere. We chose this height because it corresponds to the center of the flux rope. Computing the quasi-separatrix layers at a height above the photosphere, instead of the photosphere itself, also ensures that solution is less sensitive to boundary conditions.

Note that the QSL structure of the non-linear force free field differs significantly from that of the potential field. These differences occur not only in regions where strong electric currents are present (compare with Figure 2), but also in regions with weaker currents near the ends of the flux rope (e.g., in lower-left quadrant of Figure 3). The key point is that the presence of a coronal flux rope can dras-

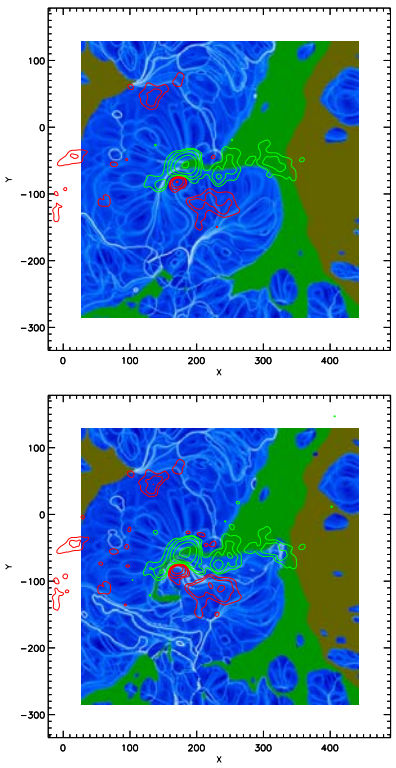

Fig. 3. Top: Quasi-separatrix layers calculated from a potential field model of AR 10930; Bottom: Quasi-separatrix layers calculated from a non-linear force-free field model of AR 10930.

tically alter the topology of the coronal field and therefore the structure of the quasi-separatrix layers.

5. Conclusion

In general, we find energies on the order of 3×10^{32} ergs and helicities on the order of 10^{43} Maxwells[2], somewhat larger than the values found by Gary et al. (1987); Bleybel et al. (2002); Régnier et al. (2002) and Mandrini et al. (2004).

We observe magnetic fields with a complex topology: there are many quasi-separatrix surfaces within the flux rope. Electric currents, that are not resolved in the present models, likely build along these quasi-separatrix layers. Magnetic reconnection and plasma heating may take place at the quasi-separatrix layers, explaining some of the observed coronal heating in the active regions.

In the future, we plan to construct such models for several Hinode XRT-observed active regions to create a statistically significant sample of models to analyze.

Acknowledgements Hinode is a Japanese mission developed and launched by ISAS/JAXA, with NAOJ as domestic partner and NASA and STFC (UK) as international partners. It is operated by these agencies in co-operation with ESA and NSC (Norway). US members of the XRT team are supported by NASA contract NNM07AA02C to SAO.

References

Berger, M. A., & Field, G. B. 1984, Journal of Fluid Mechanics, 147, 133
Bleybel, A., Amari, T., van Driel-Gesztelyi, L., & Leka, K. D. 2002, A&A, 395, 685
Bobra, M. G., van Ballegooijen, A. A., & DeLuca, E. E. 2007, ApJ, Submitted.
Canfield, R. C., Hudson, H. S., & McKenzie, D. E. 1999, Geophys. Res. Lett., 26, 627
Chae, J., Wang, H., Qiu, J., Goode, P. R., Strous, L., & Yun, H. S. 2001, ApJ, 560, 476
Gary, G. A., Moore, R. L., Hagyard, M. J., & Haisch, B. M. 1987, ApJ, 314, 782
Golub, L., et al. 2007, Sol. Phys., In press.
Hood, A. W., & Priest, E. R. 1981, Sol. Phys., 73, 289
Karpen, J. T., Tanner, S. E. M., Antiochos, S. K., & DeVore, C. R. 2005, ApJ, 635, 1319
Kuperus, M., & Raadu, M. A. 1974, A&A, 31, 189
Low, B. C., & Hundhausen, J. R. 1995, ApJ, 443, 818
Mandrini, C. H., Démoulin, P., van Driel-Gesztelyi, L., & López Fuentes, M. C. 2004, Ap&SS, 290, 319
Martin, S. F. 1998, Sol. Phys., 182, 107
Metcalf, T. R., et al. 2007, Sol. Phys., Submitted.
Pneuman, G. W. 1983, Sol. Phys., 88, 219
Priest, E. R., & Forbes, T. G. 2002, A&A Rev., 10, 313
Priest, E. R, Hood, A. W. & Anzer, U. 1989, ApJ, 344, 1010
Régnier, S., Amari, T., & Kersalé, E. 2002, A&A, 392, 1119
Rust, D. M., & Kumar, A. 1994, Sol. Phys., 155, 69
Rust, D. M., & Kumar, A. 1996, ApJL, 464, L199
Schrijver, C. J., DeRosa, M. L., Title, A. M., & Metcalf, T. R. 2005, ApJ, 628, 501
Sterling, A. C., Hudson, H. S., Thompson, B. J., & Zarro, D. M. 2000, ApJ, 532, 628
Titov, V. S., & Démoulin, P. 1999, A&A, 351, 707
Török, T., Kliem, B., & Titov, V. S. 2004, A&A, 413, L27
van Ballegooijen, A. A. 2004, ApJ, 612, 519
van Ballegooijen, A. A., & Mackay, D. H. 2007, ApJ, 659, 1713
van Ballegooijen, A. A., & Martens, P. C. H. 1989, ApJ, 343, 971
van Ballegooijen, A. A., Priest, E. R., & Mackay, D. H. 2000, ApJ, 539, 983